Methanol Synthesis from Sustainable Feedstocks – A Quantitative Side Product Analysis

Florian Nestler*, Johannes Voß, Anna Fastabend, Tammarat Niemeier, Holger Ruland and Max J. Hadrich

Supporting Information available online

Methanol synthesis from sustainable feedstocks will play an important role in the future's energy system. To enable an accurate design of crude methanol distillation systems, detailed knowledge about the amounts of side products in crude methanol is required. In this study, crude methanol samples obtained from four experimental setups covering a wide range of process conditions were analyzed for their main and side compounds. By means of a Spearman correlation analysis, the amount of carbon oxides in the reactor feed was identified as determining for the formation of side products. Trend lines describing the amount of side products were derived from the experimental data to enable studies on the downstream treatment of crude methanol.

1 Introduction

Methanol from sustainable feedstocks, i.e., atmospheric or biogenic carbon dioxide (CO_2) and carbon-neutral hydrogen (H_2), is predicted to be a key molecule in green energy transition due to its ability to substitute fossil resources such as coal, oil, and gas [1–3]. Currently, methanol and its derivates are discussed as fuels for so-called hard-to-abate sectors such as shipping and aviation [4]. Moreover, tomorrow's chemical industry will continue to rely on methanol for carbon-based products such as polymers, solvents, or organic acids [5].

To address the transformation of methanol production from fossil feedstocks towards sustainable resources, methanol synthesis from CO_2-rich gas streams has been studied extensively in the last decades [6]. By collective efforts of the scientific community, many technology-related issues such as stable and active catalyst materials [7–12], advanced process designs [13, 14], or dynamic process description [15, 16] were tackled, improved, or even resolved.

Methanol synthesis over $Cu/ZnO/Al_2O_3$ catalysts is macroscopically described by a reaction network of CO_2 hydrogenation and water-gas shift (WGS) reaction [17, 18]:

$$CO_2 + 3H_2 \rightleftarrows CH_3OH + H_2O \quad \Delta HR0 = -50 \text{ kJ mol}^{-1} \quad (1)$$

$$CO + H_2O \rightleftarrows CO_2 + H_2 \quad \Delta HR0 = -41 \text{ kJ mol}^{-1} \quad (2)$$

Both reactions are exothermic equilibrium reactions and appear at a very high selectivity. Due to the complex interplay of the reactions, understanding of the reaction kinetics remains a key challenge for an accurate description of the methanol synthesis process [19, 20]. In a previous study, Nestler et al. derived a new kinetic model applying differential temperature measurement delivering the largest set of validation data for methanol synthesis from CO_2-rich synthesis gases [21, 22].

[1]Dr. Florian Nestler https://orcid.org/0000-0003-1715-6514 (florian.nestler@ise.fraunhofer.de), [2]Johannes Voß https://orcid.org/0009-0004-8448-3595, [2]Dr. Anna Fastabend https://orcid.org/0009-0005-5968-0463, [3]Dr. Tammarat Niemeier https://orcid.org/0000-0002-5308-9083, [3]Dr. Holger Ruland https://orcid.org/0000-0001-5530-1458, [1]Max J. Hadrich https://orcid.org/0009-0002-5859-9223

[1]Fraunhofer Institute for Solar Energy Systems ISE, Sustainable Synthesis Products, Heidenhofstr. 2, 79110 Freiburg, Germany.

[2]Fraunhofer Institute for Environmental, Safety and Energy Technology UMSICHT, Low Carbon Technologies, Osterfelder Str. 3, 46047 Oberhausen, Germany.

[3]Max Planck Institute for Chemical Energy Conversion (MPI CEC), Catalytic Technology, Stiftstr. 34–36, 45470 Mülheim an der Ruhr, Germany.

Regarding overall process simulation and energy integration of the synthesis process including crude methanol distillation, multiple studies can be found in the scientific literature [13, 23–25]. Most distillation schemes involve the removal of volatile compounds, such as dissolved gases, dimethyl ether (DME) or acetone, overhead, and the removal of compounds with a higher boiling point than methanol, such as water or higher alcohols, in the sump of the distillation column. To circumvent azeotropic mixtures and to meet all required specifications, typically more than one column is necessary, which is often referred to as the topping and the refining section. To optimize the energy integration, more than two columns can be employed. The more side products are present in the distillation feed, the more theoretical stages are needed to separate the compounds due to their vapor-liquid equilibrium properties. This directly relates to the height of the distillation column and thus to the costs. Thus, a reduction in the distribution and amount of side products in crude methanol can significantly decrease the number of stages in the distillation section and thus optimized equipment size and energy consumption figures.

Zhang and co-workers executed a comprehensive analysis of multicolumn distillation setups by means of energy savings and plant economics [26]. Moreover, the authors provided a comprehensive analysis of crude methanol obtained from a conventional methanol synthesis process in their study. Recently, Shen et al. discussed the distillation system of methanol synthesis using different process configurations ranging from a single column up to an energy-integrated five-column setup with regard to energy efficiency, product purity, and heat recovery as well as design, optimization, and control strategies [27]. However, in their study no information on the amount and separation of side products is provided.

Anicic and co-workers applied a three column distillation scheme when they compared the CAMERE process, i.e., a process configuration including a reverse WGS (rWGS) pre-reactor [28], to a direct CO_2 conversion process using a synthesis loop including two reactors [29]. In their work, a three-column system was applied due to the possibility of an improved heat integration [23, 30]. As side products, methane (CH_4), DME, ethanol, and propanol were considered, however, without any information regarding the influencing parameters of their formation.

Haghighatjoo et al. performed a similar process comparison using two distillation columns, however, only considering the components water and methanol [31]. Comparing a Lurgi two-stage process concept to a single-stage concept, Rahmat et al. carried out a techno-economic and exergy analysis using a two-column distillation configuration [32]. In their simulation, the first column was used for the separation of crude methanol from dissolved gases, while the second column supposedly separated methanol and water without the presence of side products.

Because of the feed specifications from off-takers and downstream processes, the crude methanol from the synthesis section needs to be refined in most cases. On the one hand, the water content due to the synthesis of methanol from CO_2 is critical especially for the energy demand of downstream process and for thermal applications such as fuels. On the other hand, side products such as oxygenates are not tolerated due to the potential change of physical properties, such as color, smell, or reactivity.

The purity of methanol is defined by American Society for Testing and Materials (ASTM) and International Methanol Producers and Consumers Association (IMPCA) standards limiting the amount of water, acidic compounds, acetone, ethanol as well as other side products by indirect analytical parameters as, e.g., boiling point, color, odor, or density [33–35]. In order to achieve the product purities defined there, the distillation process needs to be adjusted depending on the amount of side products formed in methanol synthesis [30]. Moreover, downstream processes aiming to directly utilize crude methanol critically depend on a good understanding of side products obtained [36]. However, only few quantitative data on the composition of crude methanol exist in scientific literature.

In 1994, Göhna and König indicated a relation between the composition of the synthesis gas (syngas) and the amount of side products by means of a comprehensive analysis of crude methanol [37]. In their work, they tested a two-reactor setup fed with a CO_2-based syngas against a commercial plant fed with a syngas produced by natural gas steam reforming. The authors concluded that less trays and a lower heat demand would be necessary for the purification of CO_2-based methanol compared to its conventional counterpart. Their findings were supported by the work of Ushikoshi and co-workers analyzing the performance of a multicomponent Cu-based catalyst at reaction temperatures of 230 °C, 250 °C, and 270 °C with a pure CO_2/H_2 feed [38]. Compared to that, increased side product amounts were reported by other literature references considering synthesis gas based on conventional, CO-rich syngas [24, 26].

This publication aims to present detailed quantitative data of raw methanol samples produced using four different experimental setups over a wide range of operating conditions with a Cu-based catalyst. By means of a comprehensive correlation analysis of different process parameters towards side product formation, a basis for detailed design studies of the methanol distillation system in future work is provided.

2 Methods

2.1 Common Definitions

To characterize the composition of the make-up gas (MUG) entering the conversion process and the feed gas mixture entering the reactor (feed), the carbon oxide ratio (*COR*),

Table 1. Process data available for references providing information on the side product composition of crude methanol.

Work	No.	MUG properties	Process details	p_{syn}	T	Other comments
Göhna et al. [37]	1	$COR_{MUG} = 1.00$	Adiabatic pre-reactor with standard loop	80 bar	250.2 °C	Südchemie catalyst
	2				255.0 °C	
	3				260.1 °C	
Ushikoshi et al. [38]	4	$COR_{MUG} = 1.00$	Loop process with oil-cooled reactor	50 bar	230 °C	Tailor-made $Cu/ZnO/ZrO_2/Al_2O_3/Ga_2O_3$ catalyst; Purge rate of 1 % of inlet gas
	5	$SN_{MUG} = 2.0$			250 °C	
	6				270 °C	
Göhna et al. [37]	7	$COR_{MUG} = 0.49$[a]	Standard loop with Lurgi-type reactor	80 bar	250.0 °C	Südchemie catalyst
Zhang et al. [26]	8	$COR_{MUG} = 0.28$[a]	–	–	–	–
Supp et al. [24]	9	$COR_{MUG} = 0.21$[a]	–	–	–	–

a) Estimated using the crude methanol composition with Eq. (8).

stoichiometric number (SN), and inert gas content (y_{inert}) are defined by the molar fractions (y_i) of the respective gas components as follows [14]:

$$COR = \frac{y_{CO_2}}{y_{CO_2} + y_{CO}} \tag{3}$$

$$SN = \frac{y_{H_2} - y_{CO_2}}{y_{CO_2} + y_{CO}} \tag{4}$$

$$y_{inert} = y_{N_2} + y_{CH_4} + y_{Ar} \tag{5}$$

Due to the equilibrium limitation of methanol synthesis under technologically applied working conditions, i.e., at temperatures between 200 °C and 280 °C and pressures between 50 bar and 80 bar, unreacted gases are recycled to the reactor after crude methanol has been condensed and separated [19, 39]. The mole flow of recycled gas divided by the mole flow of MUG is defined as recycle ratio (RR) [14]:

$$RR = \frac{\dot{n}_{loop}}{\dot{n}_{MUG}} \tag{6}$$

To balance the amount of gas cycled in the process loop and prevent the accumulation of inert gases, purge gas is released through a pressure control valve. The purge fraction (PF) can be expressed by the amount of purge gas divided by the total amount of recycled process gas as follows:

$$PF = \frac{\dot{n}_{purge}}{\dot{n}_{loop}} \tag{7}$$

2.2 Available Literature Data

In Tab. 1, available literature references providing information on the composition of crude methanol for both, CO_2-based [37, 38] and conventional syngas [24, 26, 37], are listed together with the available details on the process layout and conditions. These studies will be used as external references throughout this work and are therefore considered to complement the experimental data set provided within this study. However, details on process layout and operating conditions were not entirely published

by the authors. While COR_{MUG} was provided for the processes operated with pure CO_2 [37, 38], COR_{MUG} of the conventional processes was not published. Thus, for the conventional processes, this parameter was estimated using the molar fraction of methanol (y_{MeOH}) in the crude product using the following correlation:

$$COR_{MUG} = 2 \cdot \left(1 - y_{MeOH,crude}\right) \tag{8}$$

Except for Ushikoshi et al., SN_{MUG} was given by none of the literature studies for the side product data sets. y_{inert} was provided by none of the references, however, in case of a CO_2-based MUG, $y_{inert,MUG} = 0$ can be assumed [14]. While Göhna et al. [37] and Ushikoshi et al. [38] offered further details about their process configurations, synthesis pressures (p_{syn}), synthesis temperature (T_{syn}) as well as the respective catalyst utilized, these data were not given by Zhang et al. [26] and Supp [24].

As none of the references provided more details on the process working conditions as, e.g., the feed gas parameters COR_{feed}, SN_{feed}, and $y_{inert,feed}$, these data were calculated using a process model in accordance to the information provided in the respective publications. Due to missing details on the reaction conditions, equilibrium conversion was assumed and calculated with the equilibrium constants provided by Graaf and Winkelman [40]. With exception of the CO_2-case in Göhna et al., where an adiabatic pre-reactor was utilized, a simple loop process using one reactor was presumed. Moreover, the reaction temperature provided by the authors was taken as inlet temperature for both, the adiabatic pre-reactor in case of Göhna et al. and the equilibrium reactor in the loop. Simplified flow sheets of these processes are given in Fig. S1 of the Supporting Information.

If no detailed data was provided by a reference, assumptions were made for the gas compositions in the MUG as well as the process working conditions. SN_{MUG} was set to 2.0 for all cases, while $y_{inert,MUG}$ was set to 0 % for the CO_2-based and to 5 % for the conventional processes. Unless specified otherwise, reaction pressure and temperature were set to 80 bar and 250 °C. In case of Ushikoshi et al., RR was tuned to obtain the given purge rate, i.e., amount of purge

Table 2. Specification of the experimental setups during crude methanol production by means of synthesis temperature (T) and pressure (p_{syn}) as well as gas composition (COR_{MUG}, SN_{MUG}, $y_{inert,MUG}$).

Setup	Process	T [°C]	p_{syn} [bar]	COR_{MUG}	SN_{MUG}	$y_{inert,MUG}$
(A)	Adiabatic, loop	$207 \leq X \leq 266$	51	$0.45 \leq X \leq 1.00$	$2.05 \leq X \leq 5.60$	$0.00 \leq X \leq 0.24$
(B)	Polytropic, loop	$220 \leq X \leq 273$	80	$0.09 \leq X \leq 1.00$	$2.05 \leq X \leq 2.08$	$0.00 \leq X \leq 0.22$
(C)	Isothermal, once-through	240; 250	70; 80; 85	$0.20 \leq X \leq 0.50$	$2.29 \leq X \leq 3.13$	$0.04 \leq X \leq 0.21$
(D)	Isothermal, once-through	250	85	$0.48 \leq X \leq 0.91$	$2.50 \leq X \leq 3.46$	$0.05 \leq X \leq 0.20$

gas related to the MUG, of 1 % as stated by the authors [38]. For the other simulation cases, RR was fixed to a value of 4.0. Finally, the flash temperature inside the gas/liquid separator was set to 30 °C and calculated using the Peng-Robinson equation-of-state [41] with the binary interaction parameters taken from one of our previous studies [42].

2.3 Experimental Setups and Process Conditions

Four different experimental setups (A–D) were utilized to generate crude methanol samples for analysis of trace compounds, enabling a wide range of working conditions and the interpretation of possible relations between process layout and side product formation.

Setups (A) and (B) were operated including a recycle loop for high overall syngas conversions using an adiabatic and polytropic reactor, respectively. In contrast, (C) and (D) were isothermal setups in once-through operation. All setups included a condenser to separate crude methanol from unreacted gases. Crude methanol separation from the unreacted gases was carried out at process pressure for (A) and (B), at 10 bar of pressure for setup (C), and at ambient pressures for setup (D). The liquid samples were taken from flash vessels at slightly elevated pressures and temperatures between 10 °C and 20 °C into glass sample containers at atmospheric pressure. The pressure decrease during liquid sampling could have led to losses of volatile side products. Thus, this influence needs to be considered in the discussion of the analytical results.

All experimental setups were operated with a Cu-based catalyst. Details on the process conditions during the production of the crude methanol samples considered in this work are provided in Tab. 2 for the respective experimental setups.

2.4 Sample Analysis

The crude methanol samples were analyzed by two partners applying different and complementary methods. This enables the range of detectable by-products to be increased and allows cross-checking of the different methods for validation based on compounds quantified in the corresponding analyses. The main compounds water and methanol of the raw methanol samples were determined by density measurement (Densito, Mettler Toledo). Binary mixtures with different proportions of methanol and water were prepared to determine the content of both substances based on density. The density meter recorded the temperature and density of the solutions. A correlation was established between these two parameters and the methanol content of the standard mixtures. The density and temperature of the samples were measured in the same way. The methanol concentration in the raw methanol samples was determined in comparison with the defined correlation. The water content resulted from the difference to 100 %.

By-products in the ppm range were analyzed using two different gas chromatographs coupled with a mass spectrometer (GC-MS) and high-performance liquid chromatography (HPLC). The separation on the GC system (6890N, Agilent Technologies) was performed using the capillary column DB-Wax, 60 m × 0.25 mm coated with 0.5 μm film thickness (Agilent Technologies). The oven temperature was set initially to 40 °C, held for 10 min, then increased at 10 K min^{-1} to 240 °C. The injector temperature was 230 °C. Helium was used as carrier gas at a flow rate of 3.0 mL min^{-1} in constant flow mode. The split ratio was 10:1, and 0.5 μL of sample was injected by an autosampler into the GC system. Part of the carrier gas flow was directed after the column to a quadrupole mass spectrometer (MS 5975, Agilent Technologies) and the other part to a flame ionization detector (FID). The electron impact ion source of the MS was operated in a positive mode with collision voltage and source temperature set to 70 eV and 230 °C, respectively. The data was recorded in scan mode with a mass range of 14–350 amu. The FID temperature was 250 °C. Standard solutions of different concentrations of the identified substances (dimethyl ether, methyl formate, alkanes, and alcohols) were prepared for calibration. Quantification of the analytes was done by the FID. In some cases, analytes were quantified using the calibration function of similar compounds due to the comparable FID response; as an example, 3-pentanol was evaluated via 2-pentanol.

The by-products in the crude methanol samples were further analyzed applying a Shimadzu GCMS-QP2020. 1.00 μL of the raw methanol was injected via a Shimadzu AOC-20i autosampler into an Agilent J&W CP-Wax 52 CB fused silica column (60 m × 0.25 mm × 0.25 μm) through a GC inlet at 200 °C in split mode with a split ratio of 1:50. Helium (99.999 %) was used as carrier gas at a constant column

flow of 1.50 mL min^{-1}. The GC oven temperature program was held initially at 35 °C for 4 min. Then, the temperature was increased to 220 °C with a heating rate of 20 K min^{-1}. The final temperature was held for 5 min. The GC column was connected directly to the single quadrupole MS where mass spectra of separated by-products in the range of m/z 10.00 and 300.00 were fully scanned. The temperature of the interface between GC and MS was maintained at 220 °C. Electron ionization (EI) mode was used in the MS source at a temperature of 220 °C.

The chemical compositions of the detected by-products were qualitatively identified by comparing their mass spectra to the NIST mass spectral database (National Institute of Standards and Technology, USA). The identification of major by-products, namely, ethanol, 1-propanol, 2-propanol, 1-butanol, 2-butanol, 1-pentanol, 1-hexanol, 1-heptanol, and 1-octanol, were further confirmed by comparing their retention times to those of authentic compounds. Three replicates were measured for each sample. The compounds not detected in any of the three replications or showing above 50 % uncertainty of total ion chromatogram (TIC) peak area were excluded from the by-product list. Ethanol was quantified using an external standard calibration correlating the ethanol concentrations to the integrated TIC peak areas of ethanol. The concentrations of the other by-products were estimated by their TIC with the external standard calibration for ethanol. This method is described in detail elsewhere [43, 44].

The analysis of organic acids as further by-products of methanol synthesis was carried out using HPLC-diode array detector (DAD). The HPLC system (1200 series, Agilent Technologies) was equipped with a binary gradient pump, a micro-vacuum degasser, an autosampler, a column oven, and a DAD. A Rezex ROA-Organic Acid column with hydrogen ionic form (4.6 × 250 mm, Phenomenex) was used for separation. The oven temperature was set at 60 °C. The mobile phase used was 5 mM sulfuric acid isocratic at a flow rate of 0.2 mL min^{-1}. The injection volume was 20 µL and detection with DAD was done at 210 nm. As with GC, calibration was performed using standard solutions of different concentrations. Due to the acidic eluent of the HPLC, methyl formate content of the samples was converted to formic acid during the analysis. The formic acid concentration, which arises mathematically from the methyl formate content of a sample, was therefore subtracted from the measured formic acid concentration. A complete conversion of methyl formate to formic acid was assumed for the calculation.

Table 3. Feed gas compositions (COR_{feed}, SN_{feed}, $y_{inert,feed}$), recycle ratios (RR), purge fractions (PF) as well as the adiabatic temperature rise (ΔT_{ad}) in the pre-reactor calculated by the process simulation. Values in brackets represent the feedgas composition of the adiabatic pre-reactor applied by Göhna et al. [37]. The simulation numbers refer to Tab. 1.

No.	COR_{feed}	SN_{feed}	$y_{inert,feed}$	RR	PF	ΔT_{ad}	Original ref.
1	0.83 (1.00)	10.33 (2.00)	0.00 (0.00)	4	0.74 %	35.3 K	[37]
2	0.82 (1.00)	9.55 (2.00)	0.00 (0.00)	4	0.81 %	32.1 K	[37]
3	0.82 (1.00)	8.71 (2.00)	0.00 (0.00)	4	0.90 %	28.7 K	[37]
4	0.94	10.29	0.00	4.9	0.20 %	n.a.	[38]
5	0.87	10.78	0.00	6.5	0.15 %	n.a.	[38]
6	0.76	10.76	0.00	8.7	0.11 %	n.a.	[38]
7	0.69	3.10	0.30	4	3.28 %	n.a.	[37]
8	0.54	3.13	0.34	4	2.84 %	n.a.	[26]
9	0.47	3.11	0.36	4	2.65 %	n.a.	[24]

2.5 Evaluation Methods

Numerous process parameters have been varied among the four experimental setups used in this study (compare Tab. 2). In order to identify correlations of these parameters to the formation of side products, a Spearman correlation analysis [45] was executed using the Correlation Plot app of OriginPro. As many experimental parameters, e.g., RR or weight hourly space velocity, were linked to certain experimental setups, a selection of influencing parameters was defined. These accounted to the gas composition at the reactor inlet, i.e., COR_{feed}, SN_{feed}, and $y_{inert,feed}$, as well as to p_{syn}, hotspot temperature ($T_{hotspot}$), and the catalyst's time-on-stream (ToS). A positive correlation coefficient describes an increase of a respective side product by increasing numerical parameter value and vice versa.

3 Results and Discussion

3.1 Re-simulation of Literature Data

To obtain the relevant data on the composition of the feed gas, re-simulations of the literature processes were carried out as described in Sect. 2.1. Tab. 3 lists the results obtained for the feedgas composition, recycle ratio, purge fraction as well as adiabatic temperature rise in the pre-reactor in case of working points 1–3.

For the process described by Göhna et al., the feed composition of the adiabatic pre-reactor was equal to the MUG composition (Tab. 3, No. 1–3). However, the composition of the loop reactor feed was defined by both, outlet composition of the pre-reactor and the interplay of reaction temperature and rWGS reaction in the loop. In any case, the temperature rise in the adiabatic pre-reactor was less or equal to 35 K. This result agrees with the values provided in the original publication. It is to be denoted that
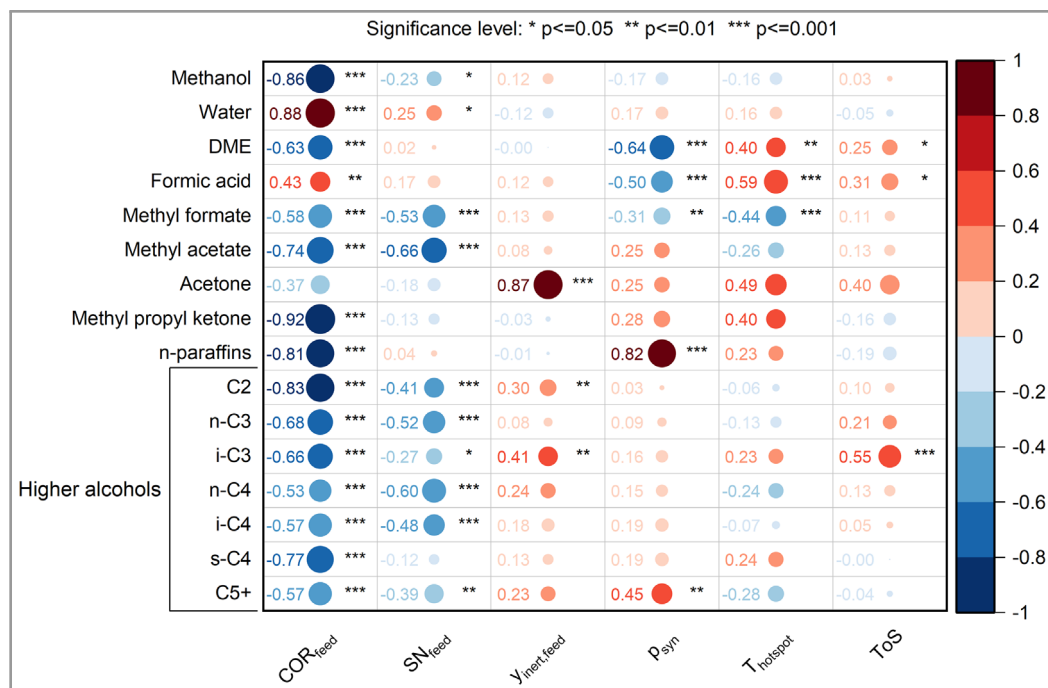
Figure 1. Correlation plot of the experimental conditions regarding the side products analyzed using the Spearman correlation. Marker sizes, colors, and values indicate the correlation coefficient obtained. Symbols (∗) denote the significance level of the correlation.

the lowest purge fraction and, hence, best conversion was achieved at the lowest reaction temperature of 250.2 °C. This can be explained by the performance of the adiabatic pre-reactor, which was highest at the lowest inlet temperature and the high equilibrium conversion of the loop reactor at this temperature.

For the re-simulation of the process proposed by Ushikoshi et al. (Tab. 3, No. 4–6), the purge rate could be held below 1 % of the inlet gas by increasing RR as stated in their study [38]. With respect to the purge fraction defined in Eq. (7), these simulations led to the lowest losses of purge gas among all simulations carried out. However, to achieve this, RR was increased from 4.9 to 8.7 as the reaction temperature was raised from 230 °C to 270 °C due to the equilibrium limitation of CO_2 hydrogenation.

The three conventional simulation scenarios (Tab. 3, No. 7–9) led to an increase of COR_{feed} compared to COR_{MUG} due to the WGS activity of the catalyst at high CO contents. The purge fractions in these cases were higher compared to the CO_2-based scenarios due to the inert gases accumulating in the loop.

The feed gas compositions for all literature references were calculated successfully. However, it is to be denoted that these values carry uncertainties due to missing process data in the original publications and the consequential assumptions necessary for the simulations (see Sect. 2.1). Thus, the re-simulated literature values provide a rough estimate rather than exact values. Still, this data will be used in

this work as reference for the side products measured during the experimental campaign in this work.

3.2 Correlations of Side Product Analyses

To evaluate the influence of the process working conditions to the formation of methanol and water as well as side products, a calculation of Spearman correlation coefficients was carried out. In Fig. 1, a correlation plot including all compounds detected in the crude methanol samples with more than ten quantitative measurements is shown over gas composition, reactor pressure, hotspot temperature, and ToS. The graph indicates a strong correlation between COR_{feed} and the amount of methanol and water with a correlation coefficient of –0.86 and 0.88, respectively, at a high significance ($p \leq 0.001$). This finding underlines the increase of water formation at increased COR and proves the plausibility of the experimental data obtained.

With exception of formic acid, a negative correlation to COR_{feed} was calculated for all side products. The compounds acetone and formic acid showed low correlation coefficients of –0.37 and 0.43, respectively. Stronger correlations (>0.53) with a high significance level ($p \leq 0.001$) appeared for the other side products. The positive influence towards the selectivity in methanol synthesis on Cu-based catalysts was already documented by other researchers [37, 46, 47]. Thus, this finding is in line with available

scientific literature. The positive correlation between COR_{feed} and the amount of formic acid in the crude methanol indicates a possible enhancement of this compound at increased CO_2 contents in the reactor feed. This, however, should be verified by further measurements, as a high scattering of the data was observed, especially at high COR_{feed}. The amount of formic acid ranged between 0 and 410 ppm with a mean value of 90.1 ppm among all samples where this compound could be analyzed. Due to the high variation of the experimental data regarding formic acid, no strong correlation was found between COR_{feed} and formic acid content in the crude methanol. Nevertheless, formic acid should be considered for crude methanol handling and purification [33, 35]. One possibility could be to consider the mean content of formic acid independently of COR_{feed}. Future experimental work could be carried out to identify a better correlation of formic acid formation and the reaction conditions. Besides formic acid, no detectable amount of other acid compounds as, e.g., acetic acid was found.

In case of acetone, only concentrations below 12 ppm were detected. As acetone was found only in a minority of the samples, further data would be necessary to provide a profound correlation for this side product.

While a strong correlation between side product formation and COR_{feed} was noticed, weaker correlations were found regarding SN_{feed} and $y_{inert,feed}$. The results of the analysis suggest that more side products are formed at lower stoichiometry and higher inert gas fractions. However, due to the multidimensional variation of process conditions, more experimental data are required to verify these influences. Similar conclusions were drawn regarding p_{syn}, $T_{hotspot}$, and ToS, as only weak correlations at low significance levels could be obtained. In the next section, the experimental data will be analyzed with a focus on COR_{feed} to derive trends for side product formation depending on this parameter.

In Fig. 2, the molar fractions of methanol and water obtained from the experiments are plotted over COR_{MUG}, color-coded for the respective experimental setups with the dashed lines providing the theoretical level of methanol and water inside the crude methanol at stoichiometric conversion (compare Eq. (8)). Experimental data for the molar fractions of methanol and water show some deviations from the theoretical values indicating possible effects due to non-equilibrium reaction conditions, losses of CO_2 in the raw methanol, purge gas losses of the setups including recycle loop as well as inaccuracies due to evaporation of volatile compounds during crude methanol sampling. The latter effect is likely to be observed in case of Setup D, consistently showing too low methanol molar fractions compared to the theoretical level. However, these low methanol molar fractions in the crude methanol could also be based on kinetic effects.
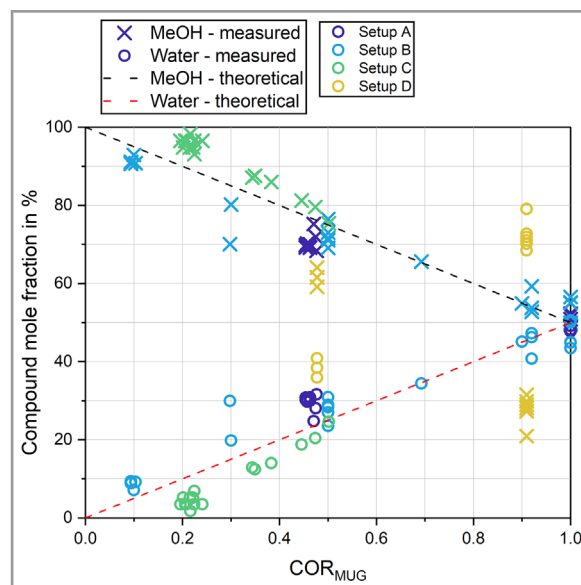

Figure 2. Molar fraction for methanol (x) and water (o) in the crude methanol samples over COR_{MUG}. Markers indicate the experimentally obtained data, while dashed lines show the theoretical composition of the crude methanol depending on the stoichiometry of the MUG.

3.3 COR Correlation of Carbonaceous Side Products

As a strong correlation between the formation of carbonaceous side products and COR_{feed} was identified from the data obtained from the experiments and literature, these correlations are further investigated within this section. In Fig. 3, the side products associated to COR_{feed} by a correlation coefficient greater than 0.5 at a high significance level ($p \leq 0.001$, compare Fig. 1) are plotted over COR_{feed}. The colors of the markers in the diagrams indicate, whether the data was obtained with one of the experimental setups or from literature, respectively. While COR_{feed} for the experimental data was directly measured, this parameter was calculated with respect to Sect. 3.1 for the literature data. Overall, the experimental data show a decreasing trend of the side products with increasing COR_{feed}. Besides some outliers, all experimental data are within the range obtained from scientific literature (yellow markers). Although the experimental data indicate trends over COR_{feed}, some noise can be identified. This is explained by multiple influences such as different experimental conditions, sampling procedures, and analytical methods (compare Sect. 2.2). More experimental data would be necessary to identify the mechanisms of side product formation.

With the aim to provide a rough correlation to the formation of the side products, an exponential function with the
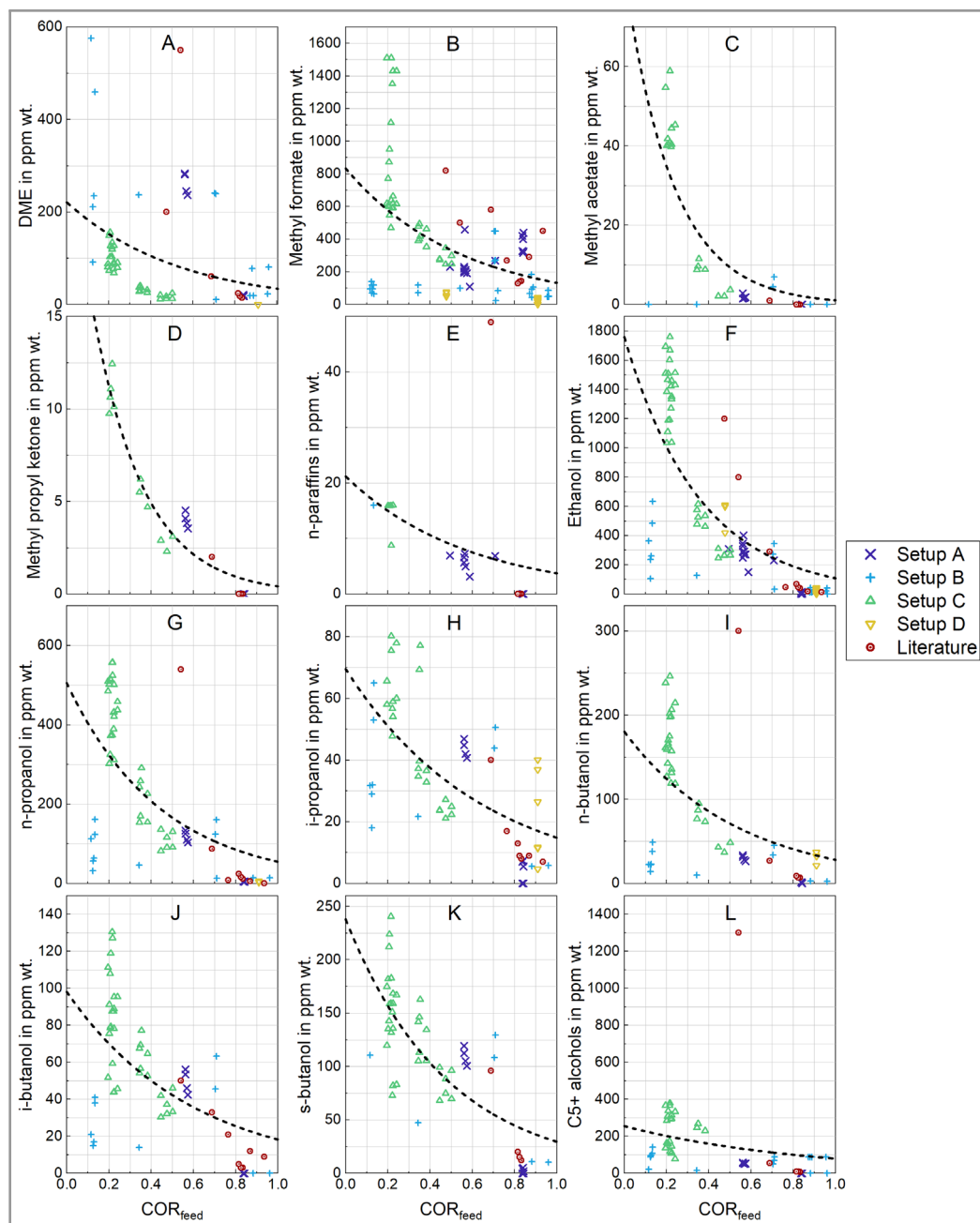
Figure 3. Side product content in the crude methanol for dimethyl ether (DME, A), methyl formate (B), methyl acetate (C), methyl propyl ketone (D), *n*-paraffins (E), ethanol (F), n-propanol (G), *i*-propanol (H), *n*-butanol (I), *i*-butanol (J), *s*-butanol (K) as well as C5+ alcohols (L). Marker colors indicate the experimental setups, the dotted lines indicate an exponential fit for the side product over COR_{feed}. Trend lines were fitted to an exponential equation with the structure $x_{\text{side product}} = a \cdot \exp(b \cdot COR_{feed})$.

following structure was fitted to the data:

$$x_{\text{side product}} = a \cdot \exp(b \cdot COR_{feed}) \qquad (9)$$

In Tab. 4, the parameters of the fitted exponential trend lines are provided. Due to the missing consideration of other influencing parameters such as SN_{feed}, $y_{\text{inert,feed}}$, p_{syn}, and reaction temperature or ToS, the description of the experimental data cannot deliver a final model, but rather a rough estimation. Nevertheless, based on the data available from the experimental campaign carried out within this study, the exponential trend lines provide an improvement to the

Table 4. Parameters for the exponential trend lines to describe side product formation related to COR_{feed}.

Compound	Parameter	Value
DME	a	221.1 ppm-wt.
	b	−1.86
Methyl formate	a	834.4 ppm-wt.
	b	−1.83
Methyl acetate	a	83.7 ppm-wt.
	b	−4.37
Methyl propyl ketone	a	25.5 ppm-wt.
	b	−4.13
n-Paraffins	a	21.2 ppm-wt.
	b	−1.73
Ethanol	a	1760.1 ppm-wt.
	b	−2.78
i-Propanol	a	69.6 ppm-wt.
	b	−1.55
n-Propanol	a	505.2 ppm-wt.
	b	−2.22
i-Butanol	a	98.1 ppm-wt.
	b	−1.68
n-Butanol	a	180.6 ppm-wt.
	b	−1.86
s-Butanol	a	238.1 ppm-wt.
	b	−2.09
C5+ alcohols	a	255.3 ppm-wt.
	b	−1.17

current understanding of side product formation. These could be considered in future studies dealing with the design of methanol distillation systems. However, further experimental points should be added to obtain a better description of the data and derive multidimensional correlations combined with the other influencing parameters. To provide a platform for expansion of the experimental data set, the raw data provided in Fig. 1 are listed in Tab. S1 of the Supporting Information of this publication.

4 Conclusion and Outlook

A systematic analysis of 96 crude methanol samples from four experimental setups operated over a wide range of working conditions was carried out by means of the main and side products formed on a Cu-based catalyst. A comparison of the experimental results to available literature indicated the validity of the analytical methods and the experiments. By a Spearman correlation analysis, COR_{feed} was identified as the most relevant process parameter for the

formation of carbonaceous side products. With exception of formic acid, the amount of all side products decreased when the CO_2 content in the reactor feed was increased, indicating a simpler purification of CO_2-based crude methanol in comparison to conventional crude methanol.

Trend lines describing side product formation related to COR_{feed} were fitted to the experimental data to provide rough estimations on their formation over Cu-based methanol synthesis catalysts. These trend lines can be applied to improve the design of methanol distillation systems and deliver an important step towards the description of quantitative side product formation. In future studies, these simplified models can be elaborated further by means of the addition of more experimental data and the integration of factors as stoichiometry, inert gas content, pressure, temperature, or ToS. Furthermore, kinetic investigations could be carried out to obtain an improved understanding of the influencing factors of side formation in methanol synthesis and to deliver more detailed models on their formation.

Supporting Information

Supporting Information for this article can be found under DOI: https://doi.org/10.1002/cite.202400009.

Symbols used

a	[ppm-wt.]	trend line parameter
A_R	[m^2]	cross-sectional area
b	[−]	trend line parameter
COR	[−]	carbon oxide ratio
m	[kg]	mass
p_{syn}	[bar]	synthesis pressure
p	[−]	p-value
PF	[−]	purge fraction
RR	[−]	recycle ratio
SN	[−]	stoichiometric number

T	[°C]	temperature
x	[–]	mass fraction
X	[variable unit]	parameter
y	[–]	mole fraction

Greek letters

Δ	difference

Sub- and Superscripts

ad	adiabatic
Ar	argon
cat	catalyst
CH_4	methane
CO	carbon monoxide
CO_2	carbon dioxide
crude	crude product
feed	reactor feed
H_2	hydrogen
hotspot	hotspot
i	component
inert	inert component
loop	recycle loop
MeOH	methanol
MUG	make-up gas
N_2	nitrogen
purge	purge gas

Abbreviations

ASTM	American Society for Testing and Materials
DAD	diode array detector
EI	electron ionization
FID	flame ionization detector
GC	gas chromatograph(y)
HPLC	high-performance liquid chromatography
IMPCA	International Methanol Producers and Consumers Association
MS	mass spectrometer
MUG	make-up gas
NIST	National Institute of Standard and Technology
rWGS	reverse water-gas shift
TIC	total ion chromatogram
ToS	time-on-stream
WGS	water-gas shift

References

[1] N. Mengis, A. Kalhori, S. Simon, C. Harpprecht, L. Baetcke, E. Prats-Salvado, C. Schmidt-Hattenberger, A. Stevenson, C. Dold, J. Zohbi, M. Borchers, D. Thrän, K. Korte, E. Gawel, T. Dolch, D. Heß, C. Yeates, T. Thoni, T. Markus, E. Schill, M. Xiao, F. Köhnke, A. Oschlies, J. Förster, K. Görl, M. Dornheim, T. Brinkmann, S. Beck, D. Bruhn, Z. Li, B. Steuri, M. Herbst, T. Sachs, N. Monnerie, T. Pregger, D. Jacob, R. Dittmeyer, *Earth's Future* **2022**, *10* (*2*), e2021EF002324. DOI: https://doi.org/10.1029/2021EF002324

[2] A. C. Løvenskiold, X. Hu, W. Zhao, F. Cherubini, *Geogr. Sustainability* **2022**, *3* (*4*), 347–357. DOI: https://doi.org/10.1016/j.geosus.2022.11.004

[3] C. Hepburn, E. Adlen, J. Beddington, E. A. Carter, S. Fuss, N. Mac Dowell, J. C. Minx, P. Smith, C. K. Williams, *Nature* **2019**, *575* (*7781*), 87–97. DOI: https://doi.org/10.1038/s41586-019-1681-6

[4] F. Ueckerdt, C. Bauer, A. Dirnaichner, J. Everall, R. Sacchi, G. Luderer, *Nat. Clim. Change* **2021**, *11* (*5*), 384–393. DOI: https://doi.org/10.1038/s41558-021-01032-7

[5] http://dechema.de/Low_carbon_chemical_industry.html

[6] S. Mbatha, R. C. Everson, N. M. Musyoka, H. W. Langmi, A. Lanzini, W. Brilman, *Sustainable Energy Fuels* **2021**, *5*, 3490–3569. DOI: https://doi.org/10.1039/D1SE00635E

[7] P. Schwiderowski, H. Ruland, M. Muhler, *Curr. Opin. Green Sustainable Chem.* **2022**, *38*, 100688. DOI: https://doi.org/10.1016/j.cogsc.2022.100688

[8] J. Zhong, X. Yang, Z. Wu, B. Liang, Y. Huang, T. Zhang, *Chem. Soc. Rev.* **2020**, *49* (*5*), 1385–1413. DOI: https://doi.org/10.1039/C9CS00614A

[9] J. Sehested, *J. Catal.* **2019**, *371*, 368–375. DOI: https://doi.org/10.1016/j.jcat.2019.02.002

[10] R. Guil-López, N. Mota, J. Llorente, E. Millán, B. Pawelec, J. L. G. Fierro, R. M. Navarro, *Materials* **2019**, *12* (*23*), 3902. DOI: https://doi.org/10.3390/ma12233902

[11] I. U. Din, M. S. Shaharun, M. A. Alotaibi, A. I. Alharthi, A. Naeem, *J. CO2 Util.* **2019**, *34*, 20–33. DOI: https://doi.org/10.1016/j.jcou.2019.05.036

[12] J. Schittkowski, H. Ruland, D. Laudenschleger, K. Girod, K. Kähler, S. Kaluza, M. Muhler, R. Schlögl, *Chem. Ing. Tech.* **2018**, *90* (*10*), 1419–1429. DOI: https://doi.org/10.1002/cite.201800017

[13] V. Dieterich, A. Buttler, A. Hanel, H. Spliethoff, S. Fendt, *Energy Environ. Sci.* **2020**, *13* (*10*), 3207–3252. DOI: https://doi.org/10.1039/D0EE01187H

[14] F. Nestler, M. Krüger, J. Full, M. J. Hadrich, R. J. White, A. Schaadt, *Chem. Ing. Tech.* **2018**, *90* (*10*), 1409–1418. DOI: https://doi.org/10.1002/cite.201800026

[15] S. Mucci, A. Mitsos, D. Bongartz, *Comput. Chem. Eng.* **2023**, *175*, 108260. DOI: https://doi.org/10.1016/j.compchemeng.2023.108260

[16] K. F. Kalz, R. Kraehnert, M. Dvoyashkin, R. Dittmeyer, R. Gläser, U. Krewer, K. Reuter, J.-D. Grunwaldt, *ChemCatChem* **2017**, *9* (*1*), 17–29. DOI: https://doi.org/10.1002/cctc.201600996

[17] J. S. Lee, K.-Y. Lee, S. Y. Lee, Y. G. Kim, *J. Catal.* **1993**, *144* (*2*), 414–424. DOI: https://doi.org/10.1006/jcat.1993.1342

[18] M. Muhler, E. Törnqvist, L. P. Nielsen, B. S. Clausen, H. Topsoe, *Catal. Lett.* **1994**, *25* (*1–2*), 1–10. DOI: https://doi.org/10.1007/BF00815409

[19] G. Bozzano, F. Manenti, *Prog. Energy Combust. Sci.* **2016**, *56*, 71–105. DOI: https://doi.org/10.1016/j.pecs.2016.06.001

[20] F. Nestler, A. R. Schütze, M. Ouda, M. J. Hadrich, A. Schaadt, S. Bajohr, T. Kolb, *Chem. Eng. J.* **2020**, *394*, 124881. DOI: https://doi.org/10.1016/j.cej.2020.124881

[21] F. Nestler, V. P. Müller, O. Salem, M. Hadrich, A. Schaadt, S. Bajohr, T. Kolb, *React. Chem. Eng.* **2021**, *6*, 1092–1107. DOI: https://doi.org/10.1039/D1RE00071C

[22] F. Nestler, *Dynamic Operation of Power-to-X Processes Demonstrated by Methanol Synthesis, Dissertation*, Engler-Bunte-Institut (EBI), *Karlsruher Institut für Technologie (KIT)* **2022**.

[23] D. S. Marlin, E. Sarron, Ó. Sigurbjörnsson, *Front. Chem.* **2018**, 6, 446. DOI: https://doi.org/10.3389/fchem.2018.00446

[24] E. Supp, *How to Produce Methanol from Coal*, Springer, Berlin **1990**.

[25] I. Dybkjær, *Chem. Econ. Eng. Rev.* **1981**, *13* (6), 17–25.

[26] J. Zhang, S. Liang, X. Feng, *Chem. Eng. Process. Process Intensif.* **2010**, *49* (10), 1031–1037. DOI: https://doi.org/10.1016/j.cep.2010.07.003

[27] Z. Shen, Q. Qu, M. Chen, H. Lyu, J. Sun, *Chem. Eng. Res. Des.* **2023**, *199*, 130–151. DOI: https://doi.org/10.1016/j.cherd.2023.09.026

[28] O.-S. Joo, *Energy Fuels* **2000**, *45* (4), 448–458.

[29] B. Anicic, P. Trop, D. Goricanec, *Energy* **2014**, *77*, 279–289. DOI: https://doi.org/10.1016/j.energy.2014.09.069

[30] M. Bertau, *Methanol: The Basic Chemical and Energy Feedstock of the Future: Asinger's Vision Today*, Springer, Berlin **2014**.

[31] F. Haghighatjoo, M. R. Rahimpour, M. Farsi, *Chem. Eng. Process. Process Intensif.* **2023**, *184*, 109264. DOI: https://doi.org/10.1016/j.cep.2023.109264

[32] Y. Rahmat, S. Maier, F. Moser, M. Raab, C. Hoffmann, J.-U. Repke, R.-U. Dietrich, *Appl. Energy* **2023**, *351*, 121738. DOI: https://doi.org/10.1016/j.apenergy.2023.121738

[33] O-M-232N, *Methanol (methyl alcohol)* **2016**.

[34] J. Ott, V. Gronemann, F. Pontzen, E. Fiedler, G. Grossmann, D. B. Kersebohm, G. Weiss, C. Witte, in *Ullmann's Encyclopedia of Industrial Chemistry*, Wiley-VCH, Weinheim **2012**.

[35] *IMPCA Methanol Reference Specifications* **2021**.

[36] M. Semmel, I. Bogatykh, B. Steinbach, J. Sauer, J.-U. Repke, O. Salem, *React. Chem. Eng.* **2023**, *8* (9), 2309–2322. DOI: https://doi.org/10.1039/D3RE00200D

[37] H. Göhna, P. König, *ChemTech* **1994**, *24* (6), 36–39.

[38] K. Ushikoshi, K. Moria, T. Watanabe, M. Takeuchi, M. Saito, *Stud. Surf. Sci. Catal.* **1998**, *114*, 357–362. DOI: https://doi.org/10.1016/S0167-2991(98)80770-2

[39] M. B. Fichtl, D. Schlereth, N. Jacobsen, I. Kasatkin, J. Schumann, M. Behrens, R. Schlögl, O. Hinrichsen, *Appl. Catal., A* **2015**, *502*, 262–270. DOI: https://doi.org/10.1016/j.apcata.2015.06.014

[40] G. H. Graaf, J. G. M. Winkelman, *Ind. Eng. Chem. Res.* **2016**, *55* (20), 5854–5864. DOI: https://doi.org/10.1021/acs.iecr.6b00815

[41] D.-Y. Peng, D. B. Robinson, *Ind. Eng. Chem. Fund.* **1976**, *15* (1), 59–64. DOI: https://doi.org/10.1021/i160057a011

[42] F. Nestler, J. Full, J.-M. Jäckle, J. Linsenmeier, J. Roob, M. J. Hadrich, A. Schaadt, *Chem. Ing. Tech.* **2022**, *94* (10), 1466–1475. DOI: https://doi.org/10.1002/cite.202200022

[43] D. Waterman, B. Horsfield, F. Leistner, K. Hall, S. Smith, *Anal. Chem.* **2000**, *72* (15), 3563–3567. DOI: https://doi.org/10.1021/ac991372x

[44] V. Ruiz-Hernández, M. J. Roca, M. Egea-Cortines, J. Weiss, *Plant Methods* **2018**, *14*, 67. DOI: https://doi.org/10.1186/s13007-018-0335-2

[45] C. Spearman, *Am. J. Psychol.* **1904**, *15* (1), 72. DOI: https://doi.org/10.2307/1412159

[46] J. Ladebeck, J. P. Wagner, T. Matsuhisa, in *Natural Gas Conversion IV*, Vol. *107*, Studies in Surface Science and Catalysis, Elsevier **1997**.

[47] M. Saito, K. Murata, *Catal. Surv. Asia* **2004**, *8* (4), 285–294. DOI: https://doi.org/10.1007/s10563-004-9119-y